Characterization of the Zirconia-Supported Tungsten Oxide System by Laser Raman and Diffuse Reflectance Spectroscopies

Delia Gazzoli,* Mario Valigi, and Roberto Dragone

Centro CNR S.A.C.S.O., c/o Dipartimento di Chimica, Università di Roma "La Sapienza", P. le A. Moro 5, I-00185 Roma, Italy

Alessandra Marucci and Giorgio Mattei

#IMAI, CNR-Area della Ricerca di Roma, P.O. Box 10, I-00016 Monterotondo Stazione, Italy

Received: June 18, 1997[⊗]

Zirconia-supported tungsten oxide samples, prepared by the equilibrium adsorption method in the pH range 2−13 by using as a support either hydrous [ZrO_2(383)] or thermally pretreated [ZrO_2(*T*)] zirconium oxide, were studied by laser Raman and diffuse reflectance spectroscopies. The W uptake increased (from ∼1.0 to ∼2.8 atoms nm^{-2}) as the pH decreased for the ZrO_2(*T*) supports, whereas for hydrous zirconia support showed the opposite trend. Different tungsten species were revealed depending on the amount of the adsorbed tungsten but not on the pH of the contacting solution. The continuous frequency shift of the Raman bands with the tungsten content, from 930 to 975 cm^{-1}, indicated the presence of monomeric species at low tungsten concentrations and of polymeric species at high loading. The uptake of the tungsten species depends on the morphology and the texture of the support.

Introduction

Supported tungsten oxide systems, mainly based on Al_2O_3, SiO_2, and TiO_2, are known to be catalytically active for an array of reactions including alcohol dehydrogenation, alkane hydrogenation, and metathesis and have been extensively investigated for both their surface and catalytic properties.[1−9] Interest has recently focused on zirconium oxide as a support because of its amphoteric properties and high thermal stability. The WO_3−ZrO_2 system, in particular, is attracting attention for acid-catalyzed reactions. Numerous studies have obtained interesting catalytic results, particularly in the hydroisomerization of alkanes, and have reported that the preparation conditions affect the nature and the strength of the active sites.[10−13] However, few papers have investigated the preparation and the characterization of this system.[14,15]

The present study deals with the preparation and the characterization of tungsten species on zirconium oxide by the equilibrium adsorption method using supports of different morphology and texture.

The equilibrium adsorption procedure is currently applied as a preparation route in our laboratory and widely used for various supported systems (Al_2O_3, SiO_2, TiO_2, and ZrO_2-supported vanadium, molybdenum, chromium, or tungsten oxides). Ample evidence shows influence of pH in controlling the uptake and the nuclearity of the adsorbed species.[16−22] For all these systems, the solution chemistry is dominated by the formation of polyoxoanions, which depends on the pH and the concentration of the solution. Several factors, including the type of support, surface coverage, thermal treatments, and extent of hydration can profoundly alter the resulting supported species. The structure of the surface species has been derived mainly from Raman spectroscopy because of the ability of this technique to identify different molecular species.[3,6−8,15,23−28] In most of the above studies, samples were thermally treated at 773 K in air but investigated under ambient conditions and thus in the presence of surface rehydration. Raman spectroscopy showed that the molecular structure of the adsorbed species paralleled that of the various species in aqueous solution, at a pH corresponding to "the net surface pH of the support at its point of zero charge (PZC)". [23]

In the present study, performed on samples dried in air at 383 K, the continuous frequency shift of the Raman bands with the tungsten content shows that the supported tungsten species depends not on the pH of the contacting aqueous solutions but on loading. The uptake of the tungsten species is also closely related to texture and morphology of the support.

Experimental Section

Sample Preparation. Hydrous zirconium oxide, hereafter designated as ZrO_2(383), was obtained by precipitation with a stream of ammonia-saturated nitrogen from a $ZrOCl_2$ solution and dried at 383 K in air for 24 h, as already reported.[20] Two sets of tungsten-containing samples were prepared. The first one is based on ZrO_2(383), and the second one is based on the hydrous zirconium oxide thermally treated in air for 5 h at the temperature *T* in the range 673−823 K, and designated as ZrO_2-(*T*). Both sets of samples were prepared by the equilibrium adsorption method, that is, by suspending a known amount of either ZrO_2(383) or ZrO_2(*T*) in a large volume of aqueous ammonium metatungstate solution, [$(NH_4)_6H_2W_{12}O_{40}$, Fluka] (AMT), at a given pH. The suspension was shaken for 72 h and the solid separated (by filtration) and dried at 383 K in air for 24 h. The solution pH was adjusted to 2 by addition of nitric acid. The addition of ammonia was used to fix the pH in the range 7−8 and to 13. The samples are designated as ZW*x*(T)*y*, where *x* stands for the analytical tungsten content (wt %), *T* for the support treatment temperature (*T* = 383, 673, 773, and 823), and *y* for the pH value recorded before the supernatant liquid was removed.

Tungsten solutions for Raman analysis were prepared by dissolving $(NH_4)_6H_2W_{12}O_{40}$ (Fluka) in water at a given pH by addition of HNO_3 or NH_3.

* Corresponding author. Fax: 0039 6 490324.

⊗ Abstract published in *Advance ACS Abstracts,* December 1, 1997.

S1089-5647(97)01999-8 CCC: $14.00

Analytical Determinations. The tungsten content was determined spectrophotometrically by the thiocyanate method at $\lambda = 400$ nm.[29,30] A weighed amount of the sample was fused with $KHSO_4$ and then dissolved in water to 50 mL. A 15 mL volume of concentrated HCl, 5 mL of $SnCl_2$, 2 mL of $TiCl_3$ freshly prepared, and then 10 mL of 15% NH_4CNS solution were added to a 10 mL aliquot of the tungsten-containing solution in a 50 mL calibrated flask. The solution was diluted to the mark and set aside for 30 min to ensure that the reaction of reduced tungsten (by $SnCl_2 + TiCl_3$) with thiocyanate ions induced full color development. The standard solution was prepared by dissolving W metal (C. Erba) with a mixture of HF and HNO_3 (1:2) and then adding 1 M NaOH to reach the final volume. The calibration curve, in the range 2−12 ppm, was obtained from standard solution of W(VI) also containing fused $KHSO_4$ in a concentration comparable to that of the samples after addition of the reagents as above.

The amount of NO_3^- ions was determined by suppressed ion chromatography.[31] The solution to be analyzed was prepared by contacting either a known amount of the sample with NaOH solution (1 M) or by dissolving the solid with HF. After filtration the pH was adjusted to ∼8 by addition of H_2SO_4. KNO_3 (Erba RPE) solutions were used as standard.

Surface Area. The sample surface areas ($S/m^2\ g^{-1}$) were measured by N_2 adsorption at 77 K (BET method). Specific surface areas, S_t, were obtained by the t-plot method for the ZrO_2(383) system.[20]

Diffuse Reflectance Spectroscopy. UV−visible spectra were recorded in the reflectance mode (R_∞) at room temperature in the range 2500−200 nm on a Cary 5E spectrophotometer, using halon as reference. To evaluate the energy bandgap (E_g) of ZWx(T)y samples as well as that of the supports and the tungsten reference compounds, the spectra were transformed to a magnitude proportional to the extinction coefficient through the Kubelka−Munk function [$F(R_\infty)$] and plotted as $\{[F(R_\infty)]*h\nu\}^2$ vs $h\nu$ ($h\nu$ = photon energy). The position of the absorption edge was determined by extrapolation of the linear portion of the curve to absorption equal zero.[32] The supported samples were normalized to the tungsten concentration of Na_2WO_4.[33]

Raman Spectroscopy. Raman spectra were collected both on solid samples and on solutions with a Spex 1877 Triplemate spectrograph equipped with an EG&G PARK liquid-nitrogen-cooled CCD-OMA detector. All solid samples, in form of pellets, were examined in back-scattering geometry by using the 514.5 nm line of an argon ion laser as the exciting source. To prevent decomposition induced by laser heating, a laser spot of 0.5 mm average diameter was used with an irradiation power not higher than 50 mW on the sample. The spectral resolution was 1.4 cm^{-1}, and the polarization of the scattered light was not analyzed. For the solutions, a 90° scattering geometry (the incident laser beam was kept parallel to the vertical edge of the entrance slit) was used with a power on the sample up to 200 mW. Spectra analysis included base line removal, smoothing, and curve fitting by a GRAMS/386 software by Galactic.

Results

Tungsten Uptake. The tungsten surface concentration (W/atoms nm^{-2}) was calculated from the analytical tungsten content and surface area values after correction for the W content.[34] The equilibrium concentration range up to $C = 0.04$ mol L^{-1} was investigated. A plot of tungsten uptake (W/atoms nm^{-2}) vs the solution equilibrium concentration (C/mol L^{-1}) is presented in Figure 1 for the ZWx(383)y samples. At pH 2 the tungsten uptake increased with the solution concentrations up to $C \approx 0.005$ mol L^{-1}. Further increases in concentration of the solution resulted in a constant uptake, about 0.35 W atoms nm^{-2}. In the pH range 7−8, the plot of the concentration vs W surface content showed a smoother trend, the saturation value being reached at about 0.5 W atoms nm^{-2}. A similar trend was observed at pH 13, the maximum W surface concentration was ∼1.0 atoms nm^{-2}.

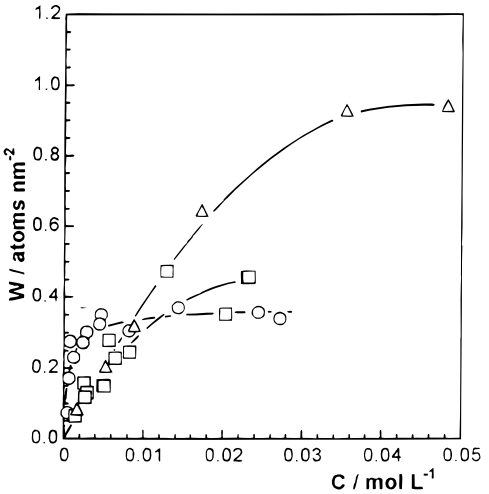

Figure 1. Tungsten surface concentration (atoms nm^{-2}) as a function of the solution equilibrium concentration (mol L^{-1}) for the ZWx(383)-y system: ○, pH 2; □, pH 8; △, pH 13.

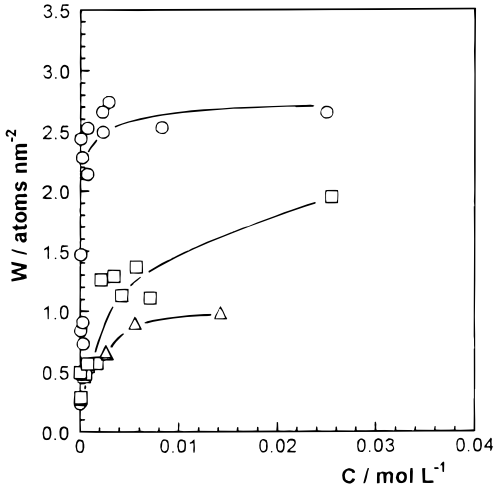

Figure 2. Tungsten surface concentration (atoms nm^{-2}) as a function of the solution equilibrium concentration (mol L^{-1}) for the ZWx(823)-y system: ○, pH 2; □, pH 8; △, pH 13.

In the ZWx(823)y samples at pH 2 the tungsten uptake increased steeply, leveling off already at $C \approx 0.002$ mol L^{-1}, with a maximum value of about 2.8 atoms nm^{-2}, Figure 2. As the pH increased to 7−8, the extent of the tungsten uptake decreased to about 1.7 atoms nm^{-2}. At pH 13 uptake again decreased, leveling off at ∼1.0 atoms nm^{-2}.

The results obtained on ZrO_2(673) and ZrO_2(773) are not drawn in graphs. The ZWx(673) samples at pH 2 showed a trend similar to that of the ZWx(383) samples (maximum uptake 0.4 atoms nm^{-2}), whereas in the pH range 7−8 they reached a higher surface content, up to 1.8 atoms nm^{-2}. In the ZWx(773) samples, prepared at pH 2 and at pH 7−8, tungsten uptake increased progressively over all the range of concentrations examined.

NO_3^- Uptake. Experiments examining the uptake of NO_3^- ions for the pure supports and for the tungsten-containing samples showed that ZrO_2(383) support had a higher NO_3^-

TABLE 1: NO_3^- Uptake for ZrO_2(*T*)*y* Supports and ZW*x*(*T*)*y* Samples

samples	S (m^2 g^{-1})	% NO_3^-	NO_3^-/atoms nm^{-2}
ZrO_2(383)2.2	330[a]	6.70[b]	1.91
ZrO_2(673)2.03	133	1.60	1.17
ZrO_2(773)1.92	76	0.95	1.21
ZrO_2(823)1.98	58	0.84[b]	1.39
ZW3.14(383)2.52	330[a]	0.26	0.08
ZW3.09(823)2.05	32	0.02	0.06

[a] S_t values. [b] Sample dissolved by HF.

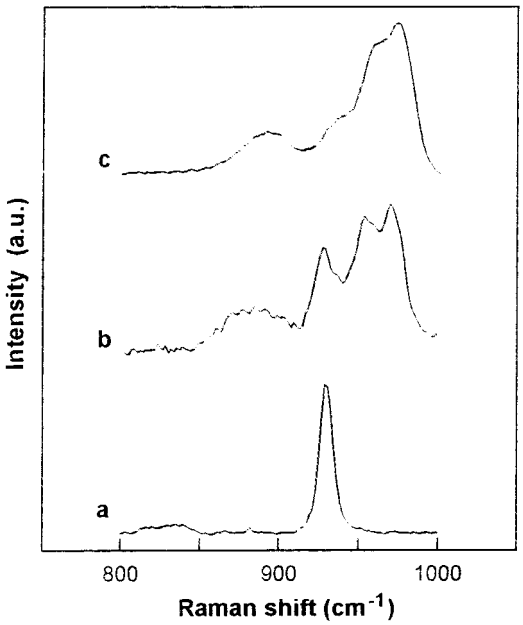

Figure 3. Raman spectra of $(NH_4)_6H_2W_{12}O_{40}$ solutions ($C \sim 3 \times 10^{-2}$ mol L^{-1}) as a function of pH: (a) pH 13; (b) pH 7.2; (c) pH 2.

surface concentration higher than the thermally treated ZrO_2-(*T*) (T = 673−823), Table 1. All the ZW*x*(T)*y* samples, irrespective of the actual thermal pretreatment of the support, exhibited a lower and practically constant uptake.

Raman Spectra

Tungsten Species in Solution. A series of solutions used for the sample preparation, were characterized as a function of pH and concentration. Figure 3 gives the Raman spectra obtained at various pH values and similar concentrations, $C \approx 3 \times 10^{-2}$ mol L^{-1}. The solution at pH 13 prepared by adding NH_3 to an AMT solution yielded a characteristic spectrum, curve a, with only two bands: a strong and sharp band at 930 cm^{-1} and a broad and weak centered around 827 cm^{-1}. The strong band can be attributed to the symmetric W═O stretching (A1) and the weak to the antisymmetric stretching (F2) of the WO_4^{2-} ions. This result agrees with previous measurements,[6,35,36] confirming that the monomeric anion is the main tungsten species present in an alkaline solution. The lowering of the pH to 7.2 led to the appearance of two new bands at about 955 and 973 cm^{-1} (curve b), whereas a further decrease in pH to 2 further shifted the bands to higher frequencies (curve c). To identify the tungsten species, the curves were fitted by mixed Gaussian−Lorentzian bands. The spectrum of the solution at pH 7.2 (Figure 3, curve b) contained components at 883, 928, 955, and 973 (Figure 4), in agreement with those of the metatungstate ion, $(H_2)W_{12}O_{40}^{6-}$,[36] and of WO_4^{2-} ions which contribute to the intensity of the 928 cm^{-1} band. The curve fitting procedure applied to the spectra of the acidic solution (Figure 3, curve c) confirmed that the main tungsten species

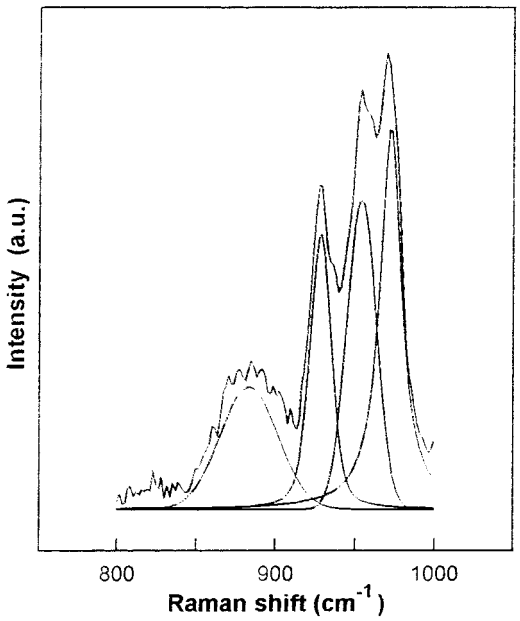

Figure 4. Curve fitting for the Raman spectrum of the $(NH_4)_6H_2W_{12}O_{40}$ solution at pH 7.2 (Figure 3b).

TABLE 2: Raman Peak Assignment for Spectra of Tungsten Species in Solution

pH ∼ 13	pH ∼ 7	pH ∼ 2	WO_4^{2-} (ref 35)	$(H_2)W_{12}O_{40}^{6-}$ (ref 36)
827 w			834 w	
	883 m	890 w		884 w
	928 s	933 w		934 w
930 vs			930 vs	
	955 s	959 s		961 s
	973 s	976 s		976 vs

present in this solution was the metatungstate ion. Table 2 collects the positions and the intensities of all band components recorded as a function of pH, together with literature data.

It was also attempted to estimate the relative Raman cross section of the $(H_2)W_{12}O_{40}^{6-}$ and WO_4^{2-} ions, by analyzing two solutions containing metatungstate (pH 2) and tungstate (pH 12) species, both with C = 0.01 mol L^{-1} in the correspondent ions. The Raman band due to the W═O vibration (in the 900−1000 cm^{-1} frequency range) for the polyanion resulted far more intense than the band of the monoanion (about eight times).

Experiments designed to investigate the effect of the W solution concentration on the Raman spectra at fixed pH in the range (3×10^{-3})−0.3 mol L^{-1} showed that at pH 13 and pH 2, the shape of the Raman spectra did not significantly depend on the concentration, although the intensity of the spectra changed. Around pH 7−8, in the presence of more complex spectra, no significant shifts in the band positions were detected, though their relative intensity changed. These results suggest that variations in the initial salt concentration, at fixed pH, lead to the same tungstate species with different relative concentrations.

The presence of zirconia on the type of the tungsten species in solution was also investigated, by examining a number of solutions collected from the suspension at the end of the adsorption step. The Raman spectra did not differ significantly from those recorded on the solutions before contact with zirconia.

Solid Samples. The ZrO_2 support exhibits no Raman features in the range 800−1100 cm^{-1}, the range of main interest for the tungsten-containing samples. Tungsten-supported specimens were examined soon after the removal of the solution (wet

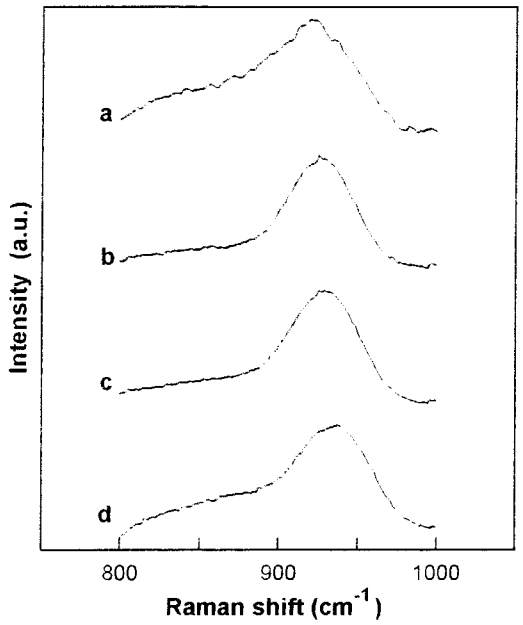

Figure 5. Raman spectra of some ZW*x*(383)*y* samples: (a) ZW1.31-(383)13; (b) ZW2.4(383)8; (c) ZW3.14(383)2; (d) ZW7.09(383)7.2.

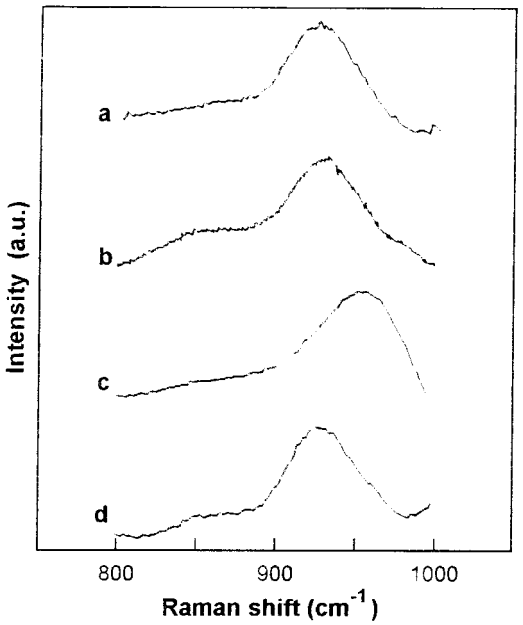

Figure 6. Raman spectra of some ZW*x*(823)*y* samples: (a) ZW0.95-(823)13; (b) ZW1.3(823)7.3; (c) ZW2.05(823)2; (d) ZW0.46(823)2.

powders), after drying in air at rt and after the standard treatment, 383 K for 24 h. Apart small differences in the intensities, no appreciable shifts in the Raman band positions were observed.

In all the ZW*x*(383)*y* samples, Figure 5, Raman spectra revealed a broad band around 930 cm^{-1}. A curve-fitting procedure showed three main bands: two weak bands centered at about 828 and 873 cm^{-1} and a strong band in the range 925−936 cm^{-1}. Inspection of Figure 5 shows that the position of this band mainly depends on the W content. As the tungsten concentration increased, the band [curve a ($x = 1.31\%$) to curve d ($x = 7.09\%$)] shifted toward high frequencies. Conversely, the pH of preparation had practically no effect: the samples having a close W concentration prepared at pH 8 (curve b) and at pH 2 (curve c) displayed similar frequencies.

In addition, the spectra of ZW*x*(383)2 samples showed a strong and narrow band at ∼1047 cm^{-1} (not shown in Figure 5), due to adsorbed NO_3^- species (from HNO_3 added to set the pH).

Spectra recorded on ZW*x*(823)*y* sample also showed a single broad band spanning the frequency range 930−975 cm^{-1}, Figure 6. The comparison of curves a, b, and c clearly indicates that the positions depended on the tungsten content: the higher the W content, the higher the frequency at which the band appears. Again, the pH of the preparation did not affect the position of the Raman bands. Samples of comparable tungsten content, but prepared at different pH (curves a and b), yielded similar position, whereas samples prepared at the same pH value (curves c and d) showed a shift to higher frequencies with W loading.

The positions of the Raman bands for the ZW*x*(383)*y* and ZW*x*(823)*y* samples, F/cm^{-1}, plotted as a function of the tungsten surface concentration, W/atoms nm^{-2} (Figure 7), yielded a linear correlation, irrespective of the preparation conditions and of the thermal treatment of the support. The ZW*x*(673)*y* and ZW*x*(773)*y* specimens also gave similar results.

Diffuse Reflectance. Figures 8 and 9 show the absorption edge, evaluated by linear extrapolation of the transformed UV−vis diffuse reflectance spectra, as a function of the W concentration (atoms nm^{-2}) for some typical ZW*x*(383)*y* and ZW*x*(823)*y* samples. They also show the values obtained for tungsten reference compounds including WO_3 (Schuchardt),

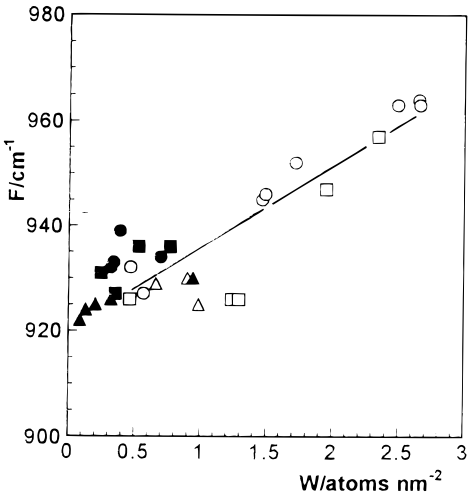

Figure 7. Raman frequencies, F/cm^{-1}, as a function of tungsten surface concentration (atoms nm^{-1}) for the ZW*x*(383)*y* and ZW*x*(823)*y* systems. ZW*x*(383)*y*: ●, pH 2; ■, pH 8; ▲, pH 13. ZW*x*(823)*y*: ○, pH 2; □, pH 8; △, pH 13.

$(NH_4)_6H_2W_{12}O_{40}\cdot 2H_2O$ (Fluka purum), and $Na_2WO_4\cdot 2H_2O$ (Kock-light Laboratories Ltd) and for the ZrO_2(383) and ZrO_2-(823) supports. The absorption edges of ZW*x*(383)*y* and ZW*x*(823)*y* samples range from 4.1 to 3.7 eV, depending on the tungsten content. Up to ∼1.0 atoms nm^{-2}, both sample sets showed fairly constant edge energies, about 4.1 eV (Figures 8 and 9). At higher tungsten concentration, the E_g values for the ZW*x*(823)*y* samples decreased towards the value characteristic of the metatungstate species (Figure 9).

Discussion

Tungsten Adsorption and Dispersion. In the equilibrium adsorption method, the adsorption process of an aqueous metal oxide species onto an oxidic support depends on the properties of the support and is related to the solution pH. The pH value determines the support surface charge and the stability of particular species in solution. As proposed by several research groups,[16−18,22] the most important factors that determine the adsorption process are the point of zero charge of the support

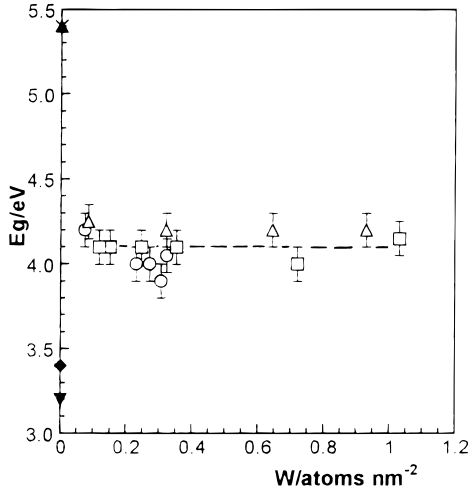

Figure 8. Absorption edge energies, E_g (eV), as a function of tungsten surface concentration (atoms cm^{-1}) for the ZW*x*(383)*y* samples, ○, pH 2; □, pH 8; △, pH 13; and reference compounds, ◆, $(NH_4)_6H_2W_{12}O_{40}$; ▲, Na_2WO_4; ×, ZrO_2(383); ▼, WO_3.

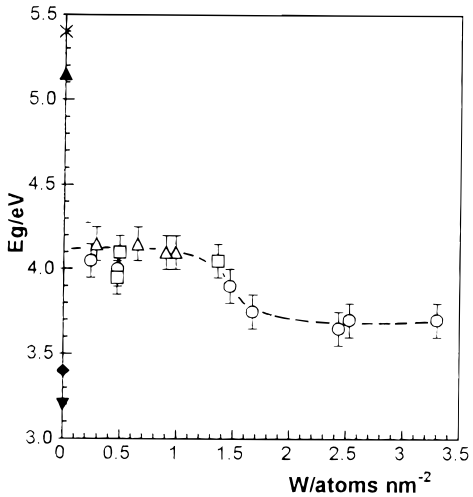

Figure 9. Absorption edge energies, E_g (eV), as a function of tungsten surface concentration (atoms cm^{-1}) for the ZW*x*(823)*y* samples, ○, pH 2; □, pH 8; △, pH 13; and reference compounds, ◆, $(NH_4)_6H_2W_{12}O_{40}$; ▲, Na_2WO_4; ×, ZrO_2(823); ▼, WO_3.

(PZC), the pH of the impregnating solution, and the nature and the charge of the species to be adsorbed. Accordingly, at a pH below the PZC of zirconia, stated to be from 4.5[37] to 6.7,[38] depending on thermal treatments and impurities, a net positive surface charge develops on the zirconia surface, thus favoring the adsorption of tungsten anionic species, whereas at a pH higher than the PZC of the support, the surface carries a negative charge and the tungsten adsorption is expected to decrease.

The tungsten anionic species, present in aqueous solution at different pH and concentration values, have been extensively studied.[39−42] It is generally accepted that, starting from a tungstate solution, above pH 8 the WO_4^{2-} ion is the only stable species, and at pH between 3.2−6.2 the tungstate solution contains $W_7O_{24}^{6-}$ ions (paratungstate A), which slowly transform into $W_{12}O_{42}H_2^{10-}$ (paratungstate B). Further acidification, between pH 3.2 and 1.0, causes metatungstate $(H_2)W_{12}O_{40}^{6-}$ species to form.[43]

In the present study the Raman analysis of solutions prepared from AMT shows that the detected species are essentially related to the pH, following the trend predicted from literature data. However, at pH 7−8, in addition to the WO_4^{2-} ions, we detected the presence of $(H_2)W_{12}O_{40}^{6-}$.

Our uptake results obtained on the ZW*x*(823)*y* samples agree with this model. According to the electrostatic model prediction, the ZW*x*(823)*y* system shows the maximum adsorption capacity at pH 2, progressively decreasing as the solution pH increases (Figure 2). Conversely, for the ZrO_2(383) based samples, the amounts of tungsten adsorbed at pH 2 and pH 7−8 were about the same, yet significantly lower than the amounts adsorbed at pH 13, Figure 1. Comparison of Figures 1 and 2 clearly shows that under the same preparation conditions (pH and solution concentration) the tungsten uptake depends on the thermal pretreatment of the support: the higher the pretreatment temperature, the higher the surface concentration.

The different adsorption trends shown by the two supports can be accounted for by their difference in texture and morphology. ZrO_2(383) is a high surface area amorphous solid ($S_t \sim 330$ m^2 g^{-1}) with a microporous structure. A determination of the pore size distribution showed a maximum at $r_p = 1.3$ nm, for radii $r_p \geq 1.0$ nm.[20] Extending the analysis to lower r_p values ($r_p \leq 1.0$ nm), it was recently found that a large fraction of the pore volume was also present in the range 0.5−1.0 nm.[44] Hence the large metatungstate anions (about 1.4 nm, as evaluated from crystallographic data of the $Mg_5H_2W_{12}O_{42}\cdot 38H_2O$ compound[45]) present in solution not only at pH 2 but also at pH 7−8 cannot have free access to the micropores of the ZrO_2(383) support. Only a small fraction of the total surface is then actually available for uptake. At pH 13 ZrO_2(383) is able to adsorb the small WO_4^{2-} species, and its uptake parallels that of ZrO_2(823) at the same pH.

The ZrO_2(823) support, prepared by thermal treatment of ZrO_2(383), is no longer microporous, because the crystallization process ($T \geq 673$ K) causes a loss of surface area and an evolution of the pores to a mesoporous structure. Hence all the surface becomes available for the adsorption of tungsten species whatever their size. Comparison of these data with those obtained in our laboratory by adsorbing chromium species at pH 2 on ZrO_2(383) and ZrO_2(823) confirms this explanation. For both supports the surface chromium concentration is in the range 2.1−2.3 Cr atoms nm^{-2} at pH 2. Although the nuclearity of the chromium species in solution depends on the pH, and the more condensed species, $Cr_2O_7^{2-}$, are present at pH about 2, their size is still smaller than the microporous radius.

On the other hand, the difference in tungsten uptake at pH 2 between the two supports can not be caused by the competitive adsorption of NO_3^- ions. In the presence of tungsten species, the NO_3^- uptake is practically constant for both sets of samples (∼0.07 atoms nm^{-2}, average value) and considerably lower than that observed for the supports (∼1.5 atoms nm^{-2}, average value).

Tungsten Species. The PZC of the support can drive the adsorption to a specific component of the solution. The final species resulting from the interaction between the support and the supported species depends, however, on complex phenomena with electrostatic and chemical contributions.

As illustrated in the results section, the Raman analysis on the tungsten containing solutions ($C \sim 10^{-1}$−10^{-3} mol/L) shows that the detected species are essentially related to the pH (Table 2). Moreover, the similarity in the spectral features of the solutions before and after contact with zirconia indicates that the presence of zirconia does not affect the nature of the tungsten species.

The spectral feature of solid samples provided less clear conclusions. The ZW*x*(383)*y* and ZW*x*(823)*y* systems lead to tungsten molecular species characterized by a broad band spanning the range 930−975 cm^{-1}. The band position is not directly related to the pH of the contacting solution (Figure 7),

but depends on the tungsten concentration. The comparison between Raman spectra of wet powders and of samples dried at 383 K in air shows only small changes in the spectral intensity, with no appreciable differences in the band position. This behavior suggests that the supported species, whatever their nature, are produced during the adsorption step and not in the drying stage. Water molecules can, indeed, play a very important role by interacting with the W surface species and causing prominent changes in the Raman spectra. As reported in the literature[3,8,15,27] and confirmed by our preliminary "in situ" experiments, the removal of water causes a shift of the Raman bands to higher frequencies. A shift of the bands from 930−975 cm^{-1} to 990−1010 cm^{-1} was recorded on ZW*x*(823)-*y* samples thermally treated at about 620 K in dry oxygen and analyzed at room temperature without exposure to the atmosphere. A subsequent exposure to ambient air restored the original spectra. Hence, here all the tungsten surface species must be considered as W oxides (monoanions as well as polyanions) interacting with coadsorbed water on the zirconia surface.

To determine the nature of the supported tungsten species contributing to the Raman spectra, we first considered samples with low tungsten content (up to ∼1 atoms nm^{-2}) and prepared from alkaline solutions. In this experimental condition the contacting solution contained only WO_4^{2-} ions, and the Raman bands at ∼930 cm^{-1} correspond to the tungstate monoanion on the zirconia surface. Because the adsorption lowers the symmetry, broadening and shifting of the Raman bands can be expected for adsorbate species, and even the appearance of new bands, e.g., infrared active bands, can be detected (the IR spectrum of some tungstate salts shows band at 850−870 cm^{-1} [7]). In the present study, frequency values around 930 cm^{-1} were also detected on samples with a W content up to ∼1.0 atoms nm^{-2}, prepared either from solution at pH 7−8 or at pH 2 in which the tungsten polyanions become the predominant species in solution. Because the Raman cross section of the metatungstate ions is larger than that of the monomeric species, the Raman bands of the metatungstate species should be not overshadowed by the stretching mode of the monomeric form. If the cross sections of the species in solution are similar to those of the adsorbed ones, our Raman analysis should reveal the replacement of the monomeric ions with the polymeric species at decreasing pH.

The fact that similar spectra are detected for all the samples characterized by a low tungsten coverage indicates that the adsorbing process on the zirconia surface leads to the formation of monoanions, independently from the tungsten species present in the preparation solutions. At increasing surface concentrations (above 1.0 atoms nm^{-2}), the main change in the Raman spectra is the shift of the W═O stretching: the higher the coverage, the higher the frequencies values. The maximum measured value is around 975 cm^{-1} for the more concentrated samples containing about 3.5 atoms nm^{-2}, pointing to the formation of an increasing fraction of polytungstate species.

To assess the nature of these adsorbates is a difficult task. Indeed, more information is needed, together with the analysis of the Raman bands associated with the W−O−W mode, appearing in the range 550−330 cm^{-1}. These bands are weak and probably detectable only on samples with a high W surface coverage. However, samples with a high surface concentration originate from zirconium oxide treated at temperatures equal or higher than those for crystallization so that the strong and complex Raman spectrum of the zirconia support makes the tungsten bands with a position lower than 800 cm^{-1} almost undetectable.

The Raman evidence is supported by the UV−visible spectra from which the bandgap energy can be estimated. As recently shown by Weber[32] for alumina-supported molybdenum systems and for a series of isopolymolybdate samples, the edge energy decreases with increasing loading and, by inference, with the average degree of aggregation. This empirical correlation gives an estimate of the degree of aggregation of the adsorbed species only and provides no information about the distribution of the species that contributes to that average. When this approach was applied to our systems it was observed a decrease in the bandgap energy values with the tungsten surface concentration for all the samples. All the samples up to ∼1.0 W atom nm^{-2} (Figures 8 and 9) had similar values and thus degrees of aggregation, whereas a further increase in the uptake resulted in more pronounced aggregation (Figure 9).

The structure of the adsorbed species, therefore, depends not on the pH of the contacting solution but on the surface concentration. Their structure may be related to the variation in the PZC of the support due to the adsorbed species. As extensively documented in literature,[19,23,46,47] the presence of impurities due to adsorption or reactions affects the PZC of an oxide system, in accordance with the PZC of the components. Because of the strong acidic properties of the tungsten compounds ($PZC_{(WO_3)}$ ∼ 0.4−1.0)[16,46], the PZC of the support is expected to decrease with the adsorption of tungsten species. At low tungsten coverage and thus at relatively high pH values, species of low nuclearity have been found, in accordance with the tungsten species properties. As the tungsten content increases, the pH at the PZC of the support decreases and the adsorbed anions start to interact with each other forming polyanion structures such as those present in aqueous solution at low pH. Therefore, at low pH values the solution contains polyanions that when adsorbed are first dissociated into monomeric units. At increasing uptake more condensed species forms.

Kohler et al.,[23] on the basis of Raman measurements, have proposed that under ambient conditions the nature of supported Mo or W species on different supports is determined by the net surface pH at the PZC. Adsorption of Mo and W, due to their acidic properties, lowers the surface pH of the oxidic support. At low Mo and W content (high pH) isolated monomeric species form, and at high surface coverage (low pH) polymeric species were detected.

A mechanism of adsorption of tungsten species on γ-Al_2O_3 from aqueous solution, in the pH range 3−10, was proposed by Karakostantis et al.[22] on the basis of the theoretical analysis of adsorption isotherms and electrochemical measurements. According to this model, in all the pH range examined, despite the large number of tungsten species existing in solution, the monomeric WO_4^{2-} anions give considerable contribution to the deposition process even in the pH range 5−3.5, being the only species in the pH range 5−3.5. These authors attributed the selective deposition of monomeric with respect to the polymeric species to the negative charge developed in the inner Helmholtz plane (IHP) of the double layer between the support surface and the contacting solution, which favors the adsorption of species with a relatively low negative charge.

The present findings clearly indicate that the nature of the tungsten species depends on the amount adsorbed. Whether the appearance of the polymeric species is due to the lowering of the pH of the support surface layer[23] or to lateral interaction between the adsorbed species as in ref 22 is still open to question. However, the lowering of the pH seems more apt to explain our results. If the adsorption process behaved selectively towards monomeric species, then the ZrO_2(383) support should

have behaved as the thermally treated one did, as found for the adsorption of small chromium species.

Conclusions

The uptake of tungsten on zirconia cannot be explained on the basis of pure electrostatic interactions between the support surface and the species in solution. The texture of the supports plays an important role in the uptake. The supported species—monomeric tungstate at low W content (∼1 W atoms nm^{-2}) and polytungstates at higher loading—are produced during the adsorption process and not in the drying stage and are highly dispersed. The difference in their structure is related not to the pH of the contacting solution but to the surface concentration.

Acknowledgment. Financial support from Italian MURST (Progetti di ricerca di interesse nazionale, 40%) is gratefully acknowleged.

References and Notes

(1) Ogata, E.; Ohta, N. *J. Catal.* **1973**, *29*, 296.
(2) Yamaguchi, T.; Tanaka, Y.; Tanabe, K. *J. Catal.* **1980**, *65*, 442.
(3) Chan, S. S.; Wachs, I. E.; Murrell, L. L.; Wang, L.; Hall, W. K. *J. Phys. Chem.* **1984**, *88*, 5831.
(4) Engweiler, J.; Harf, J.; Baiker, A. *J. Catal.* **1996**, *159*, 259.
(5) Grunert, W.; Feldhaus, R.; Anders, K.; Shpiro, E. S.; Minachev, K. M. *J. Catal.* **1989**, *120*, 444.
(6) Salvati, L.; Makovsky, L. E.; Stencel, J. M.; Brown, F. R.; Hercules, D. M. *J. Phys. Chem.* **1981**, *85*, 3700.
(7) Horsley, J. A.; Wachs, I. E.; Brown, J. M.; Via, G. H.; Hardcastle, F. D. *J. Phys. Chem.* **1987**, *91*, 4014.
(8) Stencel, J. M.; Makovsky, L. E.; Diehl, J. R.; Sarkus, T. A. *J. Raman Spectrosc.* **1984**, *15*, 282.
(9) Karakonstantis, L.; Matralis, H.; Kordulis, Ch.; Lycourghiotis, A. *J. Catal.* **1996**, *162*, 306.
(10) Hino, M.; Arata, K. *J. Chem. Soc., Chem. Commun.* **1987**, 1259.
(11) Tanabe, K.; Misono, M.; Ono, Y.; Hattori, H. *Stud. Surf. Sci. Catal.* **1989**, *51*, 5.
(12) Arata, K.; Hino, M. In *Catalysis:Theory to Practice*; Phillips, M. J., Ternan, M., Eds.; The Chemical Institute of Canada: Ontario, 1988; Vol. 4, p 1727.
(13) Larsen, G.; Lotero, E.; Parra, D. *Stud. Surf. Sci. Catal.* **1996**, *101*, 543.
(14) Zhao, B.; Xu, X.; Gao, J.; Fu, Q.; Tang, Y. *J. Raman Spectrosc.* **1996**, *27*, 549.
(15) Kim, D. S.; Ostromecki, M.; Wachs, I. E. *J. Mol. Catal. A* **1996**, *106*, 93.
(16) Brunelle, J. P. *Pure Appl. Chem.* **1978**, *50*, 1211.
(17) Wang, L.; Hall, W. K. *J. Catal.* **1982**, *77*, 232.
(18) Vermaire, D. C.; van Berge, P. C. *J. Catal.* **1989**, *116*, 309.
(19) Scierka, S. J.; Houalla, M.; Proctor, A.; Hercules, D. M. *J. Phys. Chem.* **1995**, *99*, 1537.
(20) Cimino, A.; Cordischi, D.; De Rossi, S.; Ferraris, G.; Gazzoli, D.; Indovina, V.; Minelli, G.; Occhiuzzi, M.; Valigi, M. *J. Catal.* **1991**, *127*, 744.
(21) Valigi, M.; Cimino, A.; Cordischi, D.; De Rossi, S.; Ferrari, C.; Ferraris, G.; Gazzoli, D.; Indovina, V.; Occhiuzzi, M. *Solid State Ionics* **1992**, *63*−*65*, 136.
(22) Karakonstantis, L.; Bourikas, K.; Lycourghiotis, A. *J. Catal.* **1996**, *162*, 295.
(23) Kohler, S. D.; Ekerdt, J. G.; Kim, D. S.; Wachs, I. E. *Catal. Lett.* **1992**, *16*, 231.
(24) Payen, E. *J. Raman Spectrosc.* **1986**, *17*, 233.
(25) Williams, C. C.; Ekerdt, J. G.; Jehng, J. M.; Hardcastle, F. D.; Turek, A. M.; Wachs, I. E. *J. Phys. Chem.* **1991**, *95*, 8781.
(26) Kim, D. S.; Wachs, I. E.; Segawa, K. *J. Catal.* **1994**, *146*, 268.
(27) Deo, G.; Wachs, I. E. *J. Phys. Chem.* **1991**, *95*, 5889.
(28) Kim, D. S.; Segawa, K.; Soeya, T.; Wachs, I. E. *J. Catal.* **1992**, *136*, 539.
(29) Crouthamel, C. E; Johnson, C. E. *Anal. Chem.* **1954**, *26*, 1284.
(30) Wood, D. F.; Clark, R. T. *Analyst* **1958**, *83*, 326.
(31) Small, H.; Steven, T. S.; Bauman, W. C. *Anal. Chem.* **1975**, *47*, 1801.
(32) Weber, R. S. *J. Catal.* **1995**, *151*, 470.
(33) Yang, Y.; Suna, A.; Mahler, W.; Kasawski, R. *J. Phys. Chem.* **1987**, *87*, 7315.
(34) Liu, H. C.; Weller, S. W. *J. Catal.* **1980**, *66*, 65.
(35) Ng, K. Y. S.; Gulari, E. *Polyedron* **1984**, *3*, 1001.
(36) Haufe, P. *Fresenius Z. Anal. Chem.* **1982**, *310*, 388.
(37) Crucean, E.; Rand, R. *Trans. J. Br. Ceram. Soc.* **1979**, *78*, 96.
(38) Ynoue, Y.; Yamazaki, H. *Bull. Chem. Soc. Jpn.* **1987**, *60*, 891.
(39) Titko, K. H.; Glemser, O. *Adv. Inorg. Chem. Radiochem.* **1976**, *19*, 239.
(40) Sasaki, Y.; Lindquist, I.; Sillen, L. G. *J. Inorg. Nucl. Chem.* **1959**, *9*, 93.
(41) Aveston, J.; Anacker, E. W.; Johnson, J. S. *Inorg. Chem.* **1964**, *3*, 735.
(42) Cruywagen, J. J.; van der Merwe, I. F. J. *J. Chem. Soc., Dalton Trans.* **1987**, 1701.
(43) Pope, M. T. *Heteropoly and Isopoly Oxometalates*; Springer-Verlag: Berlin, 1983.
(44) Ferraris, G. personal communication, 1996.
(45) Tsay, Y. H.; Silverstone, J. V. *Z. Kristall.* **1973**, *137*, 256.
(46) Parks, G. A. *Chem. Rev.* **1965**, *65*, 177.
(47) Subramanian, S.; Noh, J. S.; Schwarz, J. A. *J. Catal.* **1988**, *114*, 433.